GOES-12 Observations of Convective Storm Variability and Evolution During the TC4 Field Program

Kristopher M. Bedka[1] and Patrick Minnis[2]

[1]Science Systems and Applications, Inc., Hampton, VA 23666
[2]NASA Langley Research Center, Hampton, VA 23681

For *Journal of Geophysical Research* Special Issue on TC4

September 2009

Abstract

This study characterizes convective storms that occurred during the Tropical Composition, Clouds and Climate Coupling Experiment as observed within Geostationary Operational Environmental Satellite (GOES) imagery. Overshooting deep convective cloud tops (OT) that penetrate through the tropical tropopause layer (TTL) and into the stratosphere are of particular interest in this study.

The results show clear differences in the areal coverage of anvil cloud, deep convection, and OT activity over land and water and also throughout the diurnal cycle. The offshore waters of Panama, northwest Colombia, and El Salvador were the most active regions for OT-producing storms. A convective cloud object tracking system is used to monitor the duration and areal coverage of storm complexes as well as the time evolution of their cloud-top microphysical properties. The mean lifetime for these complexes is 5 hours with some existing for longer than 20 hours. Deep convection is found within the anvil cloud during 60% of the storm lifetime and covered 24% of the anvil cloud. The cloud-top height and optical depth at the storm core followed a reasonable pattern with maximum values occurring 20% into of the storm lifetime. The values in the surrounding anvil cloud peaked at relative age of 20-50% before decreasing as the convective system decays. Ice particle diameter decreased with distance from the core but generally increased with storm age. These results, which characterize the average convective system during the experiment, should be valuable for formulating and validating convective cloud process models.

1. Introduction

Recent observations have shown that stratospheric water vapor has been increasing over at least the last half century [*Oltmans et al.*, 2000; *Rosenlof et al.*, 2001], so understanding its sources and sinks is crucial for climate change studies. The 2007 Tropical Composition, Clouds and Climate Coupling Experiment (TC4) in Costa Rica was designed to address a number of questions related to the interactions among convection, clouds, and humidity in the tropical tropopause layer (TTL) and lower stratosphere [*Toon et al.*, 2009]. Changes in water vapor within the TTL can play an important role in modulating the climate since water vapor is the most powerful greenhouse gas in the atmosphere. Understanding how water behaves in the TTL is one key to better understanding the impacts of greenhouse gases on global climate change.

Overshooting deep convective cloud tops that penetrate through the TTL and into the stratosphere have been recognized as a significant source of lower stratospheric water vapor. For example, by analyzing aircraft measurements, *Dessler*, [2002] demonstrated that up to 60% of the water vapor crossing the 380 K potential temperature surface at ~ 17 km was detrained above 15 km. In a later study employing airborne measurements, *Corti et al.*, [2008], showed that ice particles from overshooting tops reached as high as 18.8 km. *Gettelman et al.* [2002] used satellite data to estimate that overshooting tops cover ~0.5% of the Tropics and penetrate up to 1.5 km into the stratosphere. *Setvak et al.* [2008] employed satellite radiances to show that mid-latitude convective storms also inject some of their water vapor into stratosphere. These and other empirical results are consistent with a variety of modeling studies (e.g., *Wang*

[2003], *Jensen et al.* [2007], *Chemel et al.* [2008]) that estimate the moisture balance of the TTL and lower stratosphere in the presence of overshooting convection.

The water vapor and ice crystals introduced into the TTL by overshooting convection are thought to be responsible for the thin, often subvisible, cirrus above 14 km in the Tropics (e.g., *Wang et al.* [1996], *Liu* [2007]). These clouds, which are characterized as having very small ice crystals (e.g., *Wang et al.* [1995]), are thought to form from a combination of effects including the direct injection of ice crystals and, more indirectly, the convective generation of gravity wave pulses that induce pileus clouds above the main convective cloud tops [*Garrett et al.*, 2006]. Fujita [1982] described these pileus clouds as "above anvil cirrus plumes." *Wang* [2007] used a cloud model to show that breaking gravity waves atop a deep convective storm can cause some water vapor to detach from the storm cloud and remain in the stratosphere. This water vapor can condense to form a cloud at levels up to 3 km above the anvil [*Levizzani and Setva*k,1996]. The above anvil cirrus clouds can extend over 100 km away from the overshooting source region (see Figure 1). However, the mechanisms that maintain these thin TTL clouds remain elusive.

Tropical convection is a diurnally driven phenomenon and, so too are the overshooting tops (OT) of deep convective clouds. It has been shown by many researchers [e.g., *Short and Wallace* [1980], *Minnis and Harrison* [1984], *Alcala and Dessler* [2002], *Liu and Zipser* [2005], *Liu et al.* [2008]) that the deepest convection over tropical land areas peaks during the late afternoon and, over ocean, during the 6 hours after local midnight. Because TC4 was designed to examine the interactions of convection and the TTL, but was limited logistically to flights only during daytime, the aircraft measurements did not sample the complete diurnal cycle. Most flights ended at or before 1600 LT, with only one mission extending to 1700 LT [*Toon et al.*, 2009]. In addition to missing a large portion of the diurnal cycle of convection, the aircraft also sampled only a small portion of each storm system that was encountered during the flights. To fill in the diurnal cycle and provide a large-scale characterization of the convection over the TC4 domain, it is necessary to employ geostationary satellite measurements. Although they do not provide the fine detail available from the in situ and remote sensing measurements aboard the aircraft, satellite measurements can be used to infer much about the context and broader implications of the aircraft data. *Minnis et al.* [2009a] provided a general overview of the clouds observed from geostationary satellites during TC4, but did not focus specifically on the properties of the convective systems over the diurnal cycles or lifetimes of the storms. Such information is important for obtaining a more comprehensive picture of TTL-convection interactions and for guiding modeling studies of tropical convection.

The purpose of this paper is to characterize deep convective storms that developed during the TC4 experiment as observed by the Twelfth Geostationary Operational Environmental Satellite (GOES-12). We seek to determine 1) the locations of frequent OT activity throughout the diurnal cycle, 2) the diurnal variability of anvil cloud, deep convective cloud, and OT areal coverage, and 3) the characteristic size and duration of individual thunderstorm complexes, and 4) the temporal evolution and spatial variability of satellite-derived cloud top properties throughout the anvil cloud during the storm lifetime. A technique exploiting the water vapor and infrared window bands of GOES-12 [*Setvak et al. 2007*] is used here to detect OTs as this method provides a direct inference of moisture transport into the TTL. The following sections describe the datasets and methodology used to conduct this study in addition to the primary results.

2. Data and Methodology

Signatures in multispectral weather satellite imagery indicate the presence of overshooting tops and moisture transport into the TTL. Overshooting tops (OTs) exhibit a lumpy or "cauliflower" textured appearance in visible and near-infrared channel imagery as they can be up to 2 km higher than the surrounding anvil cloud [*Heymsfield et al.*, 1991]. OTs are also inferred through the presence of a small cluster of very cold brightness temperatures (BTs) in the ~11 μ m infrared window (IRW) region. OTs continue to cool at a rate of 7-9 K km^{-1} as they ascend into the lower stratosphere, causing them to be significantly colder than the surrounding anvil cloud temperature [*Negri* 1982; *Adler et al.* 1983; *Bedka et al.* 2009].

The WV-IRW BTD technique, which employs the difference between the 6 - 7 μm water vapor (WV) channel BT minus the 11-μm IRW channel BT, to objectively detect OT clouds has been described extensively [*Fritz and Laszlo*, 1993; *Ackerman*, 1996; *Schmetz et al*, 1997; *Setvak et al.*, 2007; *Martin et al.*, 2008]. Generally, the brightness temperature difference (BTD) between these two channels results in a value below zero, since the WV channel weighting function usually peaks at higher altitudes and at lower temperatures than that of the IRW channel. Positive values of this BTD are shown to correspond to OTs. The reasons for this correlation are that: 1) the atmospheric temperature profile warms with height in the lower stratosphere, 2) water vapor is forced into the lower stratosphere at levels above the physical cloud top by the overshooting storm updraft, 3) this water vapor emits at the warmer stratospheric temperature whereas emission in the IR window channel originates from the colder physical cloud top, 4) positive differences between the warmer WV and colder IRW BTs can therefore reveal where overshooting is occurring. The aforementioned literature describing the WV-IRW BTD method indicates that the required WV-IRW BTD threshold for OT detection can vary depending upon satellite instrument spatial resolution and spectral channel coverage, intensity of the convective updraft, stratospheric lapse rate, and water vapor residence time in the stratosphere. For 4-km GOES imagery, a BTD value ≥ 1 K is shown to relate to the presence of overshooting [*Martin et al.*, 2008], whereas a larger value (2-3 K) is a better indicator of overshooting for higher resolution imagers [*Setvak et al.*, 2007].

2.1 Data

To characterize the diurnal variability of the convective clouds, data from half-hourly, 4-km GOES-12 imagery are analyzed over a sub-region of the greater TC4 experiment satellite domain [*Minnis et al.*, 2009a] extending from 3-18° N latitude and 77-92° W longitude. The 22-day time period, 18 July to 8 August 2007, analyzed in this study encompasses all of the TC4 tropical flight days. The 10.7-μm IRW channel pixel BTs are used to: 1) determine anvil cloud and deep convective cloud domain fractional coverage and 2) define cloud objects that are tracked from the time of first storm detection until decay. The corresponding 6.5-μm WV channel BTs are used to compute the WV-IRW BTD, which defines OT locations for this study. The GOES-12 data used in this study were provided by the University of Wisconsin-Madison Space Science and Engineering Center.

Cloud properties retrieved from the daytime GOES-12 imagery are used to characterize the micro- and macrophysical variations of the TC4 storms as they grow and decay. The parameters of interest are the cloud-top height Z_t, optical depth COD, ice crystal effective diameter D_e, and the ice water path IWP. Their values were retrieved by *Minnis et al.* [2009a] using the Visible-Infrared-Shortwave-infrared Technique (VIST), a variant of the four-channel method of *Minnis et al.* [2009b]. The post-experiment retrievals were used here. Since the VIST uses the 3.9-μm channel to retrieve D_e, the values represent the ice crystal sizes only in the upper part of the clouds. The IWP was computed as a function of D_e and OD. The method of *Minnis et al.* [2008] was used to estimate cloud-top height from IRW BT for optically thick clouds. More details of the retrievals and their errors can be found in *Minnis et al.* [2009a] and *Yost et al.* [2009].

2.2 Methodology

The satellite-observed characteristics of deep convection present during the TC4 experiment are investigated in two ways. The first method involves analysis of the fractional coverage of anvil cloud, deep convection, and overshooting top over the TC4 sub-domain described in the previous section. The purpose of this analysis is to characterize the spatial extent of deep convection and anvil cloud as well as to examine the diurnal and spatial variability of convective activity during TC4. Anvil cloud is defined by GOES-12 10.7 IRW BTs of 215-230 K, with deep convective cloud being colder than 215 K. Overshooting-top pixels are identified as those having WV-IRW BTDs ≥ 1 K. The total number of anvil, deep convection, and overshooting-top pixels are computed for each of the 48 images and the fractional coverage is computed by dividing these values by the total number of GOES-12 pixels in the domain. A set of "extremely deep convection" pixels are also defined with IRW BTs ≤ 200 K, which help to better interpret the domain areal coverage results. A 1-km terrain map is interpolated to the 4-km GOES-12 resolution and navigation and is used to separate land and ocean to understand differences in convective activity over these two surfaces.

Individual deep convective clouds are also defined as objects and are objectively tracked to determine convective cloud complex lifetime, duration of deep convection, and maximum cloud areal coverage. The Warning Decision and Support System, Integrated Information (WDSS-II, [*Lakshmanan et al.*, 2007]) is the tool used here to define and track cloud objects. The component of WDSS-II used in this study employs a hierarchical K-Means clustering method to identify storm objects at a user specified minimum spatial scale. Object motion estimation is done via pattern matching using a cross-correlation based technique. A Kalman filter is used to provide a smooth field of object movement estimates over time. *Lakshmanan et al.* [2003] provide a detailed description of the WDSS-II object definition and tracking methodology.

For this study, a "deep convective cloud" object is defined as a contiguous 25 pixel minimum area with IRW BTs ≤ 215 K. Objects are assigned an identification (ID) number by WDSS-II and object properties associated with this ID number are tracked from the time of first object detection until decay. Decay occurs when the object no longer has a sufficient area of BT ≤ 215 K. It is possible that, within the same convective storm complex and anvil cloud shield, one storm cell may be decaying and warm while another is developing nearby. Since a 215 K threshold is used to define deep convection objects, the WDSS-II system could possibly define these two cells as two objects with differing ID numbers, even though the two cells may have some relation to and interaction with each other.

Since a goal of this study is to document the characteristics of convective storm complexes during TC4, a second larger set of objects is defined that encompasses the deep convection and portions of the surrounding anvil cloud. A contiguous area having more than 50 pixels with IRW BTs ≤ 225 K is used to define these “anvil cloud” objects. Though this may seem inconsistent with the anvil cloud BT definition (215-230 K) used in the aforementioned domain areal coverage computation, experience with the WDSS-II indicates that a warmer threshold would often allow anvil clouds from distant storms to merge, producing unnaturally large objects that do not represent a single convective storm complex. When two or more deep convective cloud objects are found within one larger anvil object at the same time, the areal coverage of the two deep convection objects are combined. Characteristics associated with the object ID of the larger anvil object are monitored to maintain the time series throughout the lifetime of the storm complex.

The next component of this analysis involves analysis of the temporal evolution and spatial variability of the VIST cloud properties. The analysis begins by finding the location of the minimum IRW BT in the anvil cloud object, which is considered the “core” of the convection. Only the coldest of all objects is considered if more than one deep convection object is found within an anvil cloud object. The mean cloud top height, ice crystal effective diameter, ice water path, and optical depth are computed in a 3x3 pixel box surrounding the core. These values, rather than single-pixel values at the core, areas recorded for the 0 km radius data point. The next step is to analyze the cloud properties at increasing radius from the core. The mean cloud properties are computed within 10-km wide concentric rings at 10-km radius intervals from the storm core out to a 100 km radius. For example, the first ring would include pixels at a distance between 5 and 15 km, the second would include those from 15 to 25 km, continuing out to 100 km.

We repeat the above process for each image where the anvil object is present in the imagery. As storm complexes can exist for a wide range of time periods (1 to 12 or more hours), the time of each image where a storm is present is normalized to a number between 0 and 10, with 0 corresponding to the time of first detection and 10 corresponding to the last image before storm decay. For a storm with a lifetime of 6 images, the VIST properties from the first image are assigned to time bin 0 and those from the last image are assigned bin 10. The four remaining images are assigned to bins, 2, 4, 6, and 8, respectively, as the storm had lived 20, 40, 60, and 80% of its lifetime at each of these intervals. If a storm is present for longer than 11 images 30-min images (i.e. 5 hours), then VIST properties from multiple images could be assigned to the same bin. In this case, the data are averaged so that one data point resides in each bin. Included in this analysis are anvil cloud objects with a duration of ≥ 3 hours that existed at solar zenith angles ≤ 76°. These criteria limit our sample size to 127 out of the 877 total (to be described later) anvil cloud objects. The 76° criterion is found to minimize biases in low light conditions within the VIST algorithm. After the object lifetime is normalized, the average properties of all 127 objects are computed at each of the 11 time intervals and the 11 radii to form a composite that shows cloud temporal evolution and spatial variability throughout the storm lifetime.

3. Results and Discussion

3.1 Distribution and areal coverage of deep convection

The average diurnal variations in the domain-wide fractional coverage of anvil cloud, deep convective cloud, extremely deep convective cloud, and overshooting top are shown in Figure 2. Over land, the anvil, deep convection, and overshooting top pixels occupy the maximum area within an hour of 1800 (6 PM) local time (LT) Extremely deep convection and OT activity peaks at 1715 LT and the areal expansion of deep convective cloud continues for an hour until 1815 LT. As the storms weaken, the cloud tops warm, but convectively-induced momentum still causes the anvil cloud to expand further until it reaches its peak extent 1 hour later, on average. The pattern of OT activity mirrors that of the deep convective cloud rather than the extreme convection, as an OT can have an IRW BT > 200 K. A secondary maximum in extremely deep convection occurs between 1900 and 2100 LT while deep convection is seemingly dissipating. This will be examined in more detail below.

Over water, there is a clear maximum in extremely deep convection and OT activity during the night and early morning hours. The pattern shown by the OT line would suggest that development of intense storms occurs near 0000 LT (12 AM) and increases in coverage through 0600 LT. As the storms continue to develop, the deep convective cloud expands to peak area near 0900 LT. As these storms dissipate after 0900 LT, the convectively-induced momentum continues to expand the cloud while it decays and warms into the BT range classified as anvil cloud. The anvil cloud area peak lags that of the deep convection by 5 hours, which is longer than the lag observed over land (2 hrs). The increase in convection in coastal regions over land during the early afternoon is likely producing anvil cloud over the offshore waters. This fact, in combination with the still expanding and dissipating anvil over water, may be biasing the peak toward a later time than would occur in the absence of a convectively-active land region.

Analysis shows that 54.4% (68.1%) of land (water) OTs were present during the 9 PM to 9 AM LT period. The OT occurrences are proportionately distributed over land and ocean; 17.8% of the total OT activity occurred over land, which covers 20.4% of the domain. The greatest areal coverage of OTs over the study domain was present on 4 August and the lowest coverage was present on 24 July.

To facilitate interpretation of the patterns shown in Figure 2, Figure 3 shows the locations of OTs detected during the afternoon, evening, early morning, and late morning hours. During the afternoon, Fig. 3a shows that OT activity is most concentrated throughout the entirety of the Panama land mass and over interior regions of Costa Rica and Nicaragua. A significant concentration of OT activity is also present over the waters north of Honduras. This is caused by a series of tropical waves that moved from east to west across the northern portion of this domain during TC4. During the evening hours, OT activity was concentrated over northwest Nicaragua and the interior of Panama. The afternoon convection over Costa Rica and Panama mostly dissipated or moved westward along their Pacific coasts. The presence of convection with large areas of cold BT along the coastlines causes the areal coverage of extremely deep convection over land to increase during the 1900-2100 LT time period though the total number OTs decreased (see Figure 2).

During the early morning, OTs were abundant in the offshore and coastal regions of Colombia, Panama, and El Salvador. Animated GOES-12 IRW imagery reveals that strong convection that initially formed over northwest Colombia moved westward throughout the morning hours, triggering new development off the coasts of Panama. A similar trend is observed near El Salvador where convection that moves westward off of northwest Nicaragua helps to initiate vigorous development in the offshore waters. During late morning, the storms near Panama continue to move westward and maintain their intensity while those off of El Salvador mostly dissipate.

These results are generally consistent with previous studies that show, over tropical oceans, a broad mid-afternoon maximum in relatively weak convective cloud tops over ocean is accompanied by a second broad maximum in the most intense convection during the early morning hours (e.g., *Minnis and Harrison* [1984], *Liu and Zipser* [2005]). The peaks in the anvil, deep convective, and OT clouds over land between 1600 and 1900 LT are typical of most land areas [(e.g., *Minnis and Harrison* [1984], *Liu and Zipser* [2005]). However, the late night maximum in extremely deep convection and secondary maxima in OT and extreme deep convection over land during the early morning hours are atypical. According to Figure 3, the greatest concentration over land, during early morning, is found over the Panama-Columbia border region. *Liu et al.* [2008] found an early morning peak in precipitation over the same region indicating the extreme deep convection maximum at that time is not unusual.

3.2 Storm object analysis

The analysis will now transition to the characterization of deep convective cloud objects defined and tracked by the WDSS-II. Figure 4 shows GOES-12 visible imagery from 31 July 2007 for a complex of storms west of Costa Rica. This complex is of special interest to the TC4 experiment as the eastern portion of the cirrus anvil was well sampled by the NASA DC-8 and ER-2 aircraft. In the central portion of the domain in Figure 4a, an OT is apparent in a region of enhanced texture surrounded by a smoother anvil cloud. Extending to the east of the OT is an above-anvil cirrus plume. As noted in the Introduction, an above-anvil cirrus plume indicates the presence of water vapor in the TTL or stratosphere that has condensed to form a cirrus cloud. The plume extended ~100 km across the top of the convective storm complex by 1345 UTC (see Fig. 4c). The plume could still be seen in the 1415 UTC image (not shown) but no later due to a combination of plume dissipation and a reduction in visible channel image texture with decreasing solar zenith angle.

Figure 5 (bottom) shows that the overshooting top signatures seen in Figure 4 are well captured by the WV-IRW texture method, including the plume-producing storm. Though *Bedka et al*. [2009] and other aforementioned WV-IRW BTD references show that this method can over-diagnose the spatial coverage of OTs, the results shown here indicate that detections are isolated to the OT regions (see 1345 UTC for the best example). This adds credibility to the previously shown OT climatology and areal coverage results.

Anvil and deep convective cloud objects are also well defined in this example. The 1245 UTC panel shows two distinct deep convective areas in the northern object separated by a narrow area of warmer cloud. By 1315 UTC, the two deep convective areas merge, though the area defined by WDSS-II does not extend as far west as the cold cloud area shown in the IRW imagery. At 1345 UTC, the two anvil cloud objects come closer together and later merge into one larger object by 1415 UTC (not shown).

This storm complex was tracked by WDSS-II for a 16-hour period. Figure 6 shows the minimum IRW BT within this object throughout its lifetime. After the first 2 hours, where the storm was intensifying, the minimum BT hovered near 195 K for a period of 7 hours. Overshooting tops were detected within this complex for 10 consecutive hours. During the first 8 hours of existence, the areal coverage of the anvil and deep convection continued to expand, reaching a peak near 1500 UTC. The merger between the northern and southern storm complex in the 1345-1415 UTC time frame is evident in this plot. The results here suggest that two other mergers later occurred at 1645 and 1815 UTC. Animated IRW imagery shows that the increase in anvil cloud and deep convection area is caused by new convective initiation within this complex, which provided a new influx of cold cloud tops. Warming cloud tops and decreasing areal coverage after 1900 UTC indicates that the complex is decaying rapidly.

Since the results have shown that the WDSS-II can accurately monitor the evolution of convective complexes for long time periods, WDSS-II was applied to 30 minute imagery over the full duration of the TC4 experiment. We focus on anvil cloud objects (i.e. convective complexes) that exist longer than 30 min and are collocated with a deep convection object at least once during their lifetime. A total of 877 complexes met this criteria and are included in the following analyses. Figure 7 (top) shows that the lifetime of the 31 July object described above was in the 95th percentile of all objects tracked by WDSS-II. The mean lifetime of anvil cloud objects is 5 hours and the object contained deep convection for 3 hours (60%) of this time (not shown in Figure). Figure 7 also shows that the 31 July complex was quite large relative to other complexes that developed during TC4. The mean of the maximum areal coverage of anvil cloud objects is 13,900 km^2 and the mean of the maximum coverage of deep convection is 3345 km^2, indicating that deep convection covers 24% of a mature convective storm complex (not shown in Figure). Based upon the areal coverage of the WV-IRW BTD OT detections, it is determined that OT pixels represent only 0.15% of a convective storm complex. It is important to note here that these results are based on the anvil cloud being defined by a 225 K BT. In reality, semi-transparent anvil cloud along the periphery of a storm complex can spread and add a significant amount of areal coverage to the anvil cloud statistics, thereby reducing the mean coverage of deep convection and OT pixels.

3.3. Deep convective cloud and anvil microphysics

Areal coverage of the convective complexes constitutes only one aspect of the storm lifetime. The ice water budget of the clouds and its impact on the radiation budget are important characteristics of the convection that need to be understood if they are to be properly modeled. The influence on the radiation budget can computed using the D_e, COD, and the cloud-top temperature or Z_t, while the ice water variations can be monitored using IWP.

Figure 8 shows the mean variations of each of those parameters for 127 storms as functions of the relative age of the system and the distance from the core of the storm using the approach described earlier. The cloud-top height (Figure 8a) of the core drops by ~0.8 km during the average complex's lifetime, from 15.8 km to 15.0 km. This decrease with age extends 100 km from the storm center, but diminishes to a magnitude of less than 0.3 km at ~75 km from the storm center. The decrease is not monotonic with the peak heights occurring around 20% into life of the system.

The mean COD (Figure 8b) of the core is at a maximum of ~95 for the first half of its existence and drops by ~40% as it decays. Overall, the average COD varies non-monotonically, with mean maximum values occurring during the first 50% of the lifetime to a distance of 70 km from the core. Beyond 70 km, the youngest and oldest clouds have the greatest CODs, which are about half of the core values. The mean ice particle sizes (Figure 8c) at the core are smallest early in the storm life but generally increase with age. Within the first 20-km radius, D_e drops by 1-3 μm regardless of age. At distances between 30 and 60 km from the center, D_e is a maximum about 60% through the average storm's life. It is lowest for the new anvil at this distance range. IWP peaks at ~40% into the storm's life when COD and D_e are near or at their peak values (Figure 8d). IWP drops by a factor of 2 at 100 km from the center at the time of peak storm intensity. When the storm decays, the IWP is lowest and the drop with distance is much less pronounced due to the decreased COD and the homogeneity of D_e.

When cores penetrate the TTL, the cloud properties tend to be more extreme. For OT clouds, the mean values of COD, D_e, and Z_t are 104.6, 84.8 μm, and 16.3 km, respectively (not shown). These values can be compared to 83.2, 80.5 μm, and 15.7

km, respectively, for cores that are not classified as having OTs. By definition, the cloud tops are higher for OT storms. The increased optical depth is due in part to the greater thickness and reflects the intensity of storms, but it also reflects the age of the storms since the cores are less vigorous with age as seen in Figure 8b.

When the object can be identified with the WDSS-II, the core is still growing, reaching its peak at 20-40% into its lifetime. This peak is defined by maxima in all parameters except ice diameter. The rise and fall of Z_t follows the growth and decay of the convective system (Figure 8a). The anvil continues to build vertically until the system is in middle age. Its top then drops to lower altitudes at a faster pace than that of the growth stage. The initially smaller particles at the top of the core may be due to the rapid rise of the younger particles in the relatively dry environment above the cloud, whereas, the droplets and ice crystals ascending within the already formed convective core are in a moister environment where they can grow to larger sizes (Figure 8c). This might explain why the anvil contains significantly smaller particles early in its existence, but rapidly accumulates large ice crystals as the convection proceeds. The slower rate of decrease in D_e with increasing radius as the system decays could also be due to the greater abundance of moisture in the surrounding environment compared to the initial stages. It is not clear why D_e increases with distance beyond ~60 km for the younger clouds. Perhaps, there is some influence of other systems overlapping the younger anvils.

4. Summary and Conclusions

This study characterizes the convective storms that occurred during the TC4 field program as observed within GOES-12 10.7 μm IR window imagery. There were clear differences in the areal coverage of anvil cloud, deep convection, and overshooting top activity over land and water and also throughout the diurnal cycle. Overshooting top detections from the WV-IRW method were used to determine where this activity is most frequent across a subset of the TC4 domain.

As would be expected, convection over interior land regions increased during the 1315-1815 LT period in conjunction with strong solar heating of a humid tropical air mass. The northern coast and offshore waters of Honduras were particularly active during the 1315-2345 LT period. Northwest Nicaragua and El Salvador also showed a convective maximum within the 1845-2345 LT period. Convection developed and moved across the offshore waters and coastal areas of these two nations during the early morning hours, producing a distinct regional maximum in OT activity. The offshore waters of Panama, northwest Colombia, and El Salvador were the most active regions for OT-producing storms. The greatest areal coverage of OT activity over the study domain was present on 4 August.

A large convective storm complex that occurred on 31 July was examined in detail in this paper as the anvil cloud from this complex was well sampled by TC4 research aircraft. The 1-km visible-channel imagery showed the presence of an above-anvil cirrus plume that was evident for a 1.5 hour period. This plume was connected to a persistent overshooting top area that served to inject water vapor into the TTL and/or stratosphere that condensed to form a cloud. This large convective complex was detected and tracked for 16 hours by the WDSS-II system. The anvil cloud from this complex covered a ~65,000 km^2 area, making it one of the largest and most long-lived of those detected during the TC4 experiment. Overshooting tops were detected within this complex for 10 consecutive hours.

A total of 877 convective storm complexes were detected and tracked by WDSS-II throughout the duration of the TC4 experiment. The mean lifetime for these complexes is 5 hours with anvil cloud at its greatest horizontal extent covering a mean area of 13,900 km^2. Deep convection is found within the anvil cloud during 60% of the storm lifetime and covers 24% of the total anvil area. As most observed overshooting tops are ≤ 15 km in diameter, they only occupy 0.15% of the anvil cloud, on average. The areal coverage proportions of deep convection and overshooting are likely a bit too high because a relatively cold 225 K BT threshold is used to define the spatial extent of the anvil cloud.

The microphysical properties of convective systems were determined only for storms that occurred completely during sunlit conditions. On average, they followed a reasonable pattern with maximum values of cloud top height and optical depth occurring at the core roughly at a time corresponding to 20% of the system's lifetime. The values in the anvil peaked at relative age of 20-50% before decreasing as the convective system decayed. Ice particles decreased in size with distance from the center of the core but generally increased in size with storm age. These results, which characterize the average convective system during the experiment, should be valuable for formulating and validating convective cloud process models.

The results presented here indicate that the diurnal cycles of convective clouds and overshooting tops are quite consistent with climatology, not only over the experiment area, but also over the Tropics, in general. Thus, the TC4 aircraft measurements, when taken as a whole, should be representative of tropical convective systems. However, because they were confined to daylight flights, they did not sample most of the clouds that produce overshooting tops, the main source for TTL moisture. Nevertheless, at least, one of the most intense daytime storms (July 31) was sampled by the experiment and should provide the basis for a good case study.

It is clear that the satellite imagery is critical for learning the behavior of these complex convective systems. By bringing the knowledge gained from the satellite analyses together with the TC4 in situ data and numerical cloud process models, it should be possible to make some important strides in understanding deep convection over the Tropics and its interaction with the TTL.

Acknowledgements

This research was supported by the NASA Radiation Science Program TC4 project, the NASA Applied Sciences Program, and the Department of Energy Atmospheric Radiation Measurement Program through Interagency Agreement, DE-AI02-07ER64546. The authors thank Kirk Ayers for processing the TC4 VIST microphysical retrievals and the University of Wisconsin Space Science and Engineering Center for providing the GOES-12 data and McIDAS software support.

References

Ackerman, S.A. (1996), Global satellite observations of negative brightness temperature differences between 11 and 6.7 µm. *J. Atmos. Sci.*, **53**, 2803–2812.

Adler, R. F., M. J. Markus, D. D. Fen, G. Szejwach, and W. E. Shenk (1983), Thunderstorm top structure observed by aircraft overflights with an infrared radiometer. *J. Appl. Meteor. and Climatol*., **22**, 579-593.

Alcala, C. M. and A. E. Dessler (2002), Observations of deep convection in the tropics using the Propical Rainfall Measuring Mission (TRMM) precipitation radar, *J. Geophys. Res.*, *107*, doi:10.1029/2002JD002457.

Bedka, K. M., J. C. Brunner, R. Dworak, W. F. Feltz, J. A. Otkin, and T. Greenwald (2009), Objective satellite-based overshooting top detection using infrared window channel brightness temperature gradients. *J. Appl. Meteor. and Climatol*., In Press.

Chemel C., M. R. Russo, J. A. Pyle, R. S. Sokhi, and C. Schiller (2008), Quantifying the imprint of a severe hector thunderstorm during ACTIVE/SCOUT-O3 onto the water content in the upper troposphere/lower stratosphere. *Mon. Wea. Rev*, In Press.

Corti, T., and Co-authors (2008), Unprecedented evidence for deep convection hydrating the tropical stratosphere, *Geophys. Res. Lett.*, **35**, doi:10.1029/GL033641.

Dessler, A. E. (2002), Te effect of deep, tropical convection on the tropical tropopause layer, *J. Geophys. Res.*, **107**, doi:10.1029/2001JD000511.

Fritz, S., and I. Laszlo (1993), Detection of water vapor in the stratosphere over very high clouds in the tropics. *J. Geophys. Res.*, **98** (D12), 22959-22967.

Garrett, T. J., J. Dean-Day, C. Liu, B. K. Barnett, G. G. Mace, D. G. Baumgardner, C. R. Webster, T. P. Bui, W. G. Read, and P. Minnis (2006), Convective formation of pileus near the tropopause, *Atmos. Chem., & Phys.*, **6**, 1185-1200.

Gettelman, A., M. L. Salby, and F. Sassi (2002), Distribution and influence of convection in the tropical tropopause region, *J. Geophys. Res*., **107**, doi:10.1029/2001JD001048.

Heymsfield, G.M., R. Fulton, and J.D. Spinhirne (1991), Aircraft overflight measurements of Midwest severe storms: Implications and geosynchronous satellite interpretations. *Mon. Wea. Rev.*, **119**, 436–456.

Jensen, E. J., A. S. Ackerman, and J. A. Smith (2007), Can overshooting convection dehydrate the tropical tropopause layer? *J. Geophys. Res.*, **112**, doi:10.1029/2006JD007943.

Lakshmanan, V., T. Smith, G. Stumpf, and K. Hondl (2007), The Warning Decision Support System–Integrated Information. *Wea. Forecasting*, **22**, 596–612.

Lakshmanan, V., R. Rabin, and V. DeBrunner (2003), Multiscale storm identification and forecast. *J. Atmos. Res.*, 367-380.

Liu, C. (2007), Geographical and seasonal distribution of tropical tropopause thin clouds and their relation to deep convection and water vapor viewed from satellite measurements, *J. Geophys. Res.*, **112**, doi:10.1029/2006JD007479.

Liu, C. and E. J. Zipser (2005), Global distribution of convection penetrating the tropical tropopause, *J. Geophys. Res.*, **110**, doi:10.1029/2005JD006063.

Liu, C., E. J. Zipser, G. G. Mace, and S. Benson (2008), Implications of the differences between daytime and nighttime CloudSat observations over the tropics, J. Geophys. Res., 113, doi:10.1029/2008JD009783.

Machado, L. A. T., W. B. Rossow, R. L. Guedes, and A. W. Walker (1998), Life cycle variations of mesoscale convective systems over the Americas, *Mon. Wea. Rev*., **126,** 1630– 1654.

Martin, D. W., R. A. Kohrs, F. R. Mosher, C. M. Medaglia, and C. Adamo (2008), Over-ocean validation of the Global Convective Diagnostic. *J. Appl. Meteor. Climatol.*, **47**, 525-543.

Minnis, P. and E. F. Harrison (1984), Diurnal variability of regional cloud and clear-sky radiative parameters derived from GOES data, Part II: November 1978 cloud distributions, *J. Clim. Appl. Meteorol.*, **23**, 1012-1031.

Minnis, P. and co-authors (2009a), Cloud properties determined from GOES and MODIS data during TC4, *J. Geophys. Res*., submitted.

Minnis, P., S. Sun-Mack, and Co-authors (2009), Cloud property retrievals for CERES using TRMM VIRS and Terra and Aqua MODIS data. *IEEE Trans. Geosci. Remote Sens.*, submitted.

Minnis, P., C. R. Yost, S. Sun-Mack, and Y. Chen (2008), Estimating the physical top altitude of optically thick ice clouds from thermal infrared satellite observations using CALIPSO data, *Geophys. Res. Lett.*, *35*, L12801, doi:10.1029/2008GL033947.

Negri, A. J. (1982), Cloud-top structure of tornado storms on 10 April 1979 from rapid scan and stereo satellite observations, *Bull. Amer. Meteor. Soc.,* **63**, 1851–1859.

Oltmans, S.J., Vömel, H., Hofmann, D.J., Rosenlof, K.H., Kley, D. (2000), The increase in stratospheric water vapor from balloonborne frostpoint hygrometer measurements at Washington, D.C., and Boulder, Colorado. *Geophys. Res. Let*. **27**, 3453–3456.

Rosenlof, K.H., Oltmans, S.J., Kley, D., Rossell III, J.M., Chiou, E.W., Chu, W.P., Johnson, D.G., Kelly, K.K., Michelsen, H.A., Nedoluha, G.E., Remsberg, E.E., Toon, G.C., McCormick, M.P. (2001), Stratospheric water vapor increases over the past halfcentury. *Geophys. Res. Let*. **28**, 1195–1198.

Schmetz, J., S. A. Tjemkes, M. Gube, and L. van de Berg (1997), Monitoring deep convection and convective overshooting with METEOSAT. *Adv. Space. Res.*, **19**, 433-441.

Setvak, M., R. M. Rabin, and P. K. Wang (2007), Contribution of the MODIS instrument to observations of deep convective storms and stratospheric moisture detection in GOES and MSG imagery. *Atmos. Res*., **83**, 505-518.

Setvak, M., D. T. Lindsey, R. M. Rabin, P. K. Wang, A. Demeterova (2008), Indication of water vapor transport into the lower stratosphere above midlatitude convective storms: Meteosat Second Generation satellite observations and radiative transfer model simulations. *Atmos. Res.*, **89**, 170-180.

Short, D. A. and J. M. Wallace (1980), Satellite-inferred morning-to-evening cloudiness changes, *Mon. Wea. Rev.*, **108**, 1160-1169.

Toon, O. B. and Co-authors (2009), Planning and implementation of the Tropical Composition, Cloud and Climate Coupling Experiment (TC4), *J. Geophys. Res.*, This issue.

Wang, P.-H., P. Minnis, M. P. McCormick, G. S. Kent, and K. M. Skeens (1996), A 6-year climatology of cloud occurrence frequency from SAGE II observations (1985-1990), *J. Geophys. Res.*, **101**, 29,407-29,429.

Wang, P. K. (2003), Moisture plumes above thunderstorm anvils and their contribution to cross-tropopause transport of water vapor in midlatitudes. *J. Geophys. Res.* **108** (D6), AAC 51–AAC 515.

Wang, P. K. (2007), The thermodynamic structure atop a penetrating convective thunderstorm, *Atmos. Res*., **83**, 254–262

Yost, C. R., and Co-authors (2009), Comparison of in-situ and remotely sensed microphysical properties of deep convective clouds and anvils during TC4, *J. Geophys. Res.*, Submitted.

List of Figure Captions

Figure 1: GOES-8 channel 1, 3 and 4 composite imagery across the US Great Plains showing a row of thunderstorms with anvil top plumes (indicated by white arrows) at 0015 UTC on 06 May 2002. From Wang (2007).

Figure 2: Fractional coverage of anvil cloud, deep convective cloud, extremely deep convective cloud, and overshooting top pixels over land (top) and water (bottom) within the TC4 domain. The solid (dashed) lines correspond to the left (right) y-axis.

Figure 3: Locations of WV-IRW based OT detections over land (blue) and water (cyan) during the a) afternoon (1315-1815 LT), b) evening (1845-2345 LT), c) early morning (0015-0515 LT), and d) late morning (0545-1045 LT).

Figure 4: Contrast-enhanced GOES-12 visible channel imagery at 1315 (top) and 1345 UTC (bottom) on 31 July 2007. An overshooting top (dashed circle) is connected to an above-anvil cirrus plume (solid line) in both panels. Subpanels show the plume region in closer detail.

Figure 5: GOES-12 IRW imagery (top row), WDSS-II objects (middle row), and WV-IRW BTD based OT detections (bottom row) at 1245 (left column), 1315 (middle column), and 1345 UTC (right column) on 31 July 2007. WDSS-II objects colored blue represent anvil cloud objects identified with a 225 K IRW BT threshold. WDSS-II objects colored red represent the deep convective area IRW BT ≤ 215 K.

Figure 6: (top) The minimum IRW BT throughout the lifetime of the convective storm complex shown in Figure 5. Asterisks denote the times that OTs were detected within the object. (bottom) The areal coverage of anvil cloud and deep convection for the same object.

Figure 7: (top) The lifetime of anvil cloud (black bars) and duration of deep convection (grey bars) tracked by the WDSS-II. (bottom) The maximum anvil and deep convective cloud object areal coverage for cloud complexes tracked by the WDSS-II.

Figure 8: A temporal and spatial variability of the mean a) cloud top height, b) cloud optical depth, c) ice particle diameter, and d) ice water path for a composite of 127-storm complexes during the TC4 field experiment.

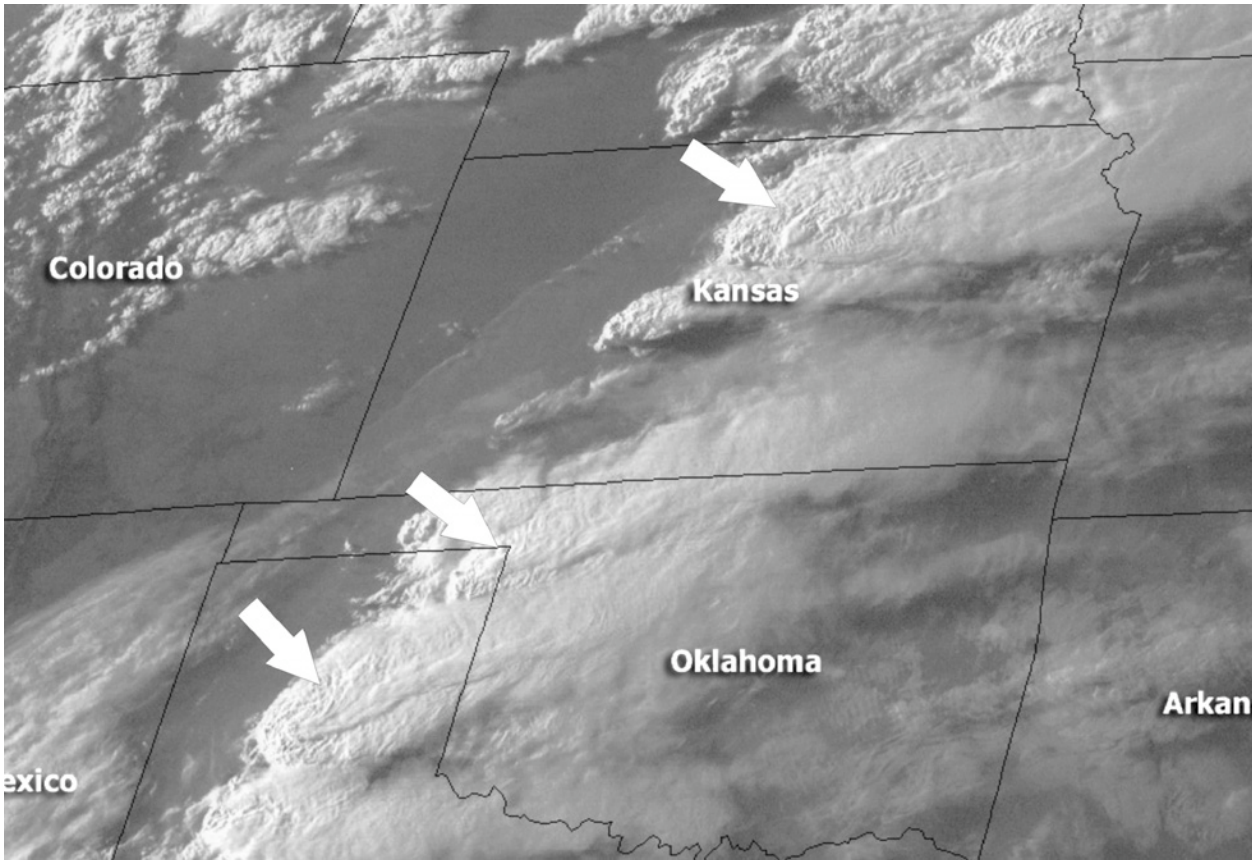

Figure 1: GOES-8 channel 1, 3 and 4 composite imagery across the US Great Plains showing a row of thunderstorms with anvil top plumes (indicated by white arrows) at 0015 UTC on 06 May 2002. From Wang (2007).

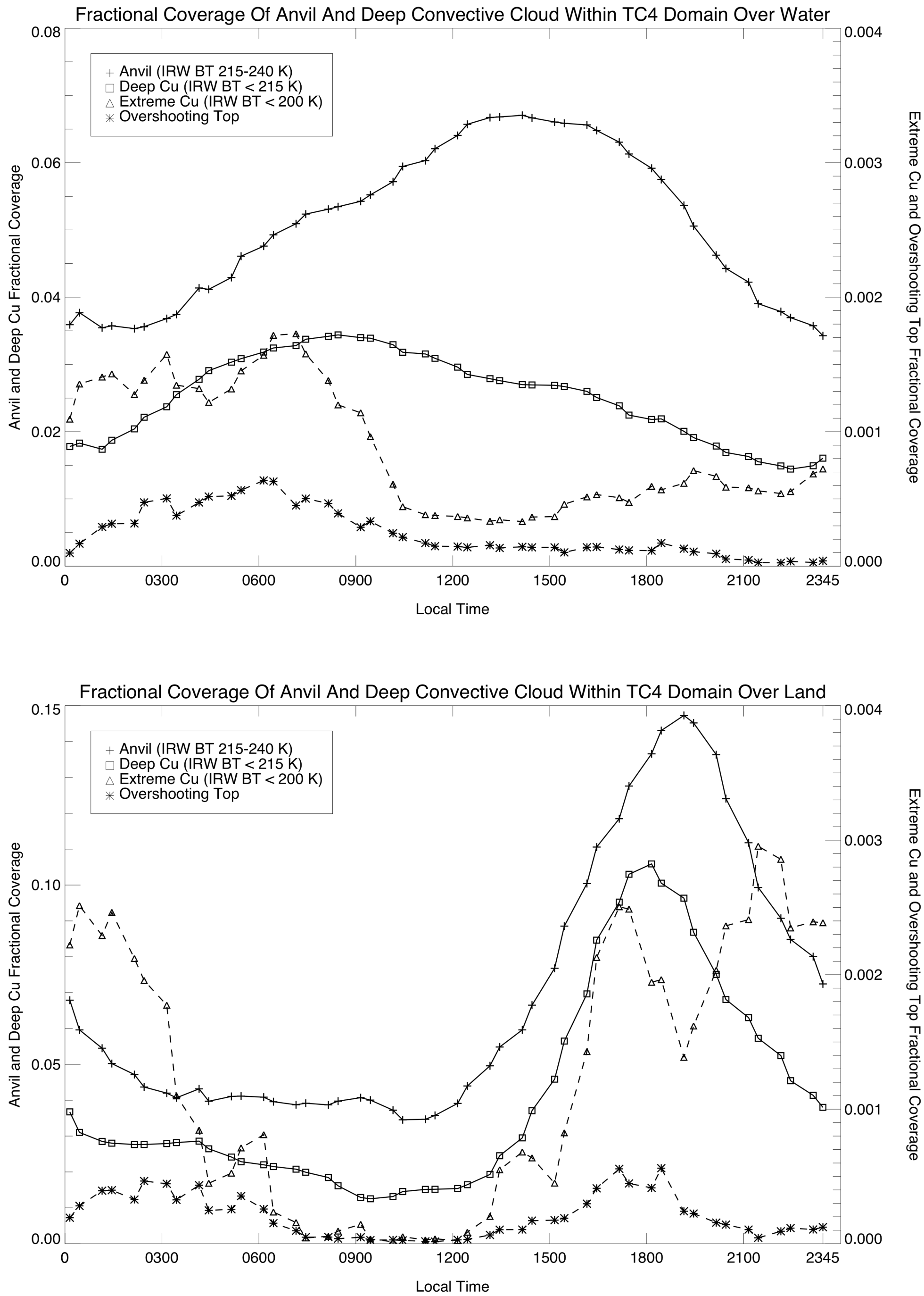

Figure 2: Fractional coverage of anvil cloud, deep convective cloud, extremely deep convective cloud, and overshooting top pixels over land (top) and water (bottom) within the TC4 domain.   The solid (dashed) lines correspond to the left (right) y-axis.

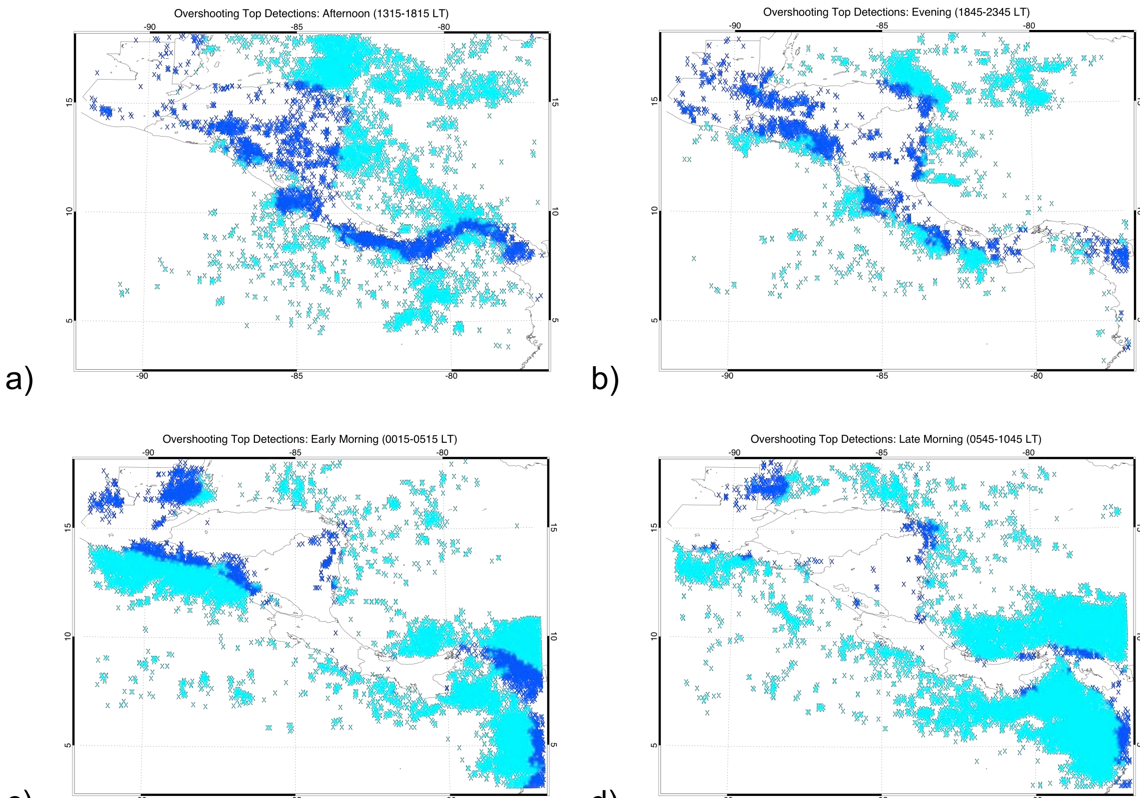

Figure 3: Locations of WV-IRW based OT detections over land (blue) and water (cyan) during the a) afternoon (1315-1815 LT), b) evening (1845-2345 LT), c) early morning (0015-0515 LT), and d) late morning (0545-1045 LT).

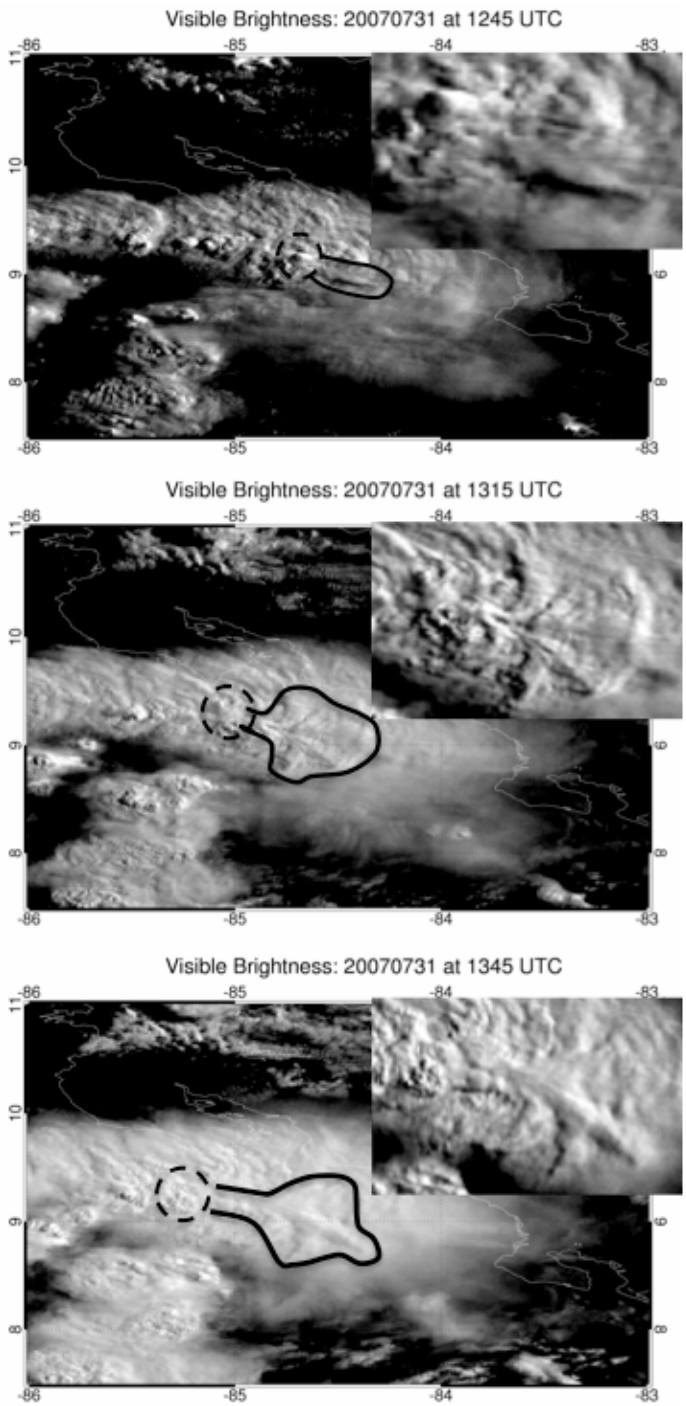

Figure 4: Contrast-enhanced GOES-12 visible channel imagery at 1315 (top) and 1345 UTC (bottom) on 31 July 2007. An overshooting top (dashed circle) is connected to an above-anvil cirrus plume (solid line) in both panels. Subpanels show the plume region in closer detail.

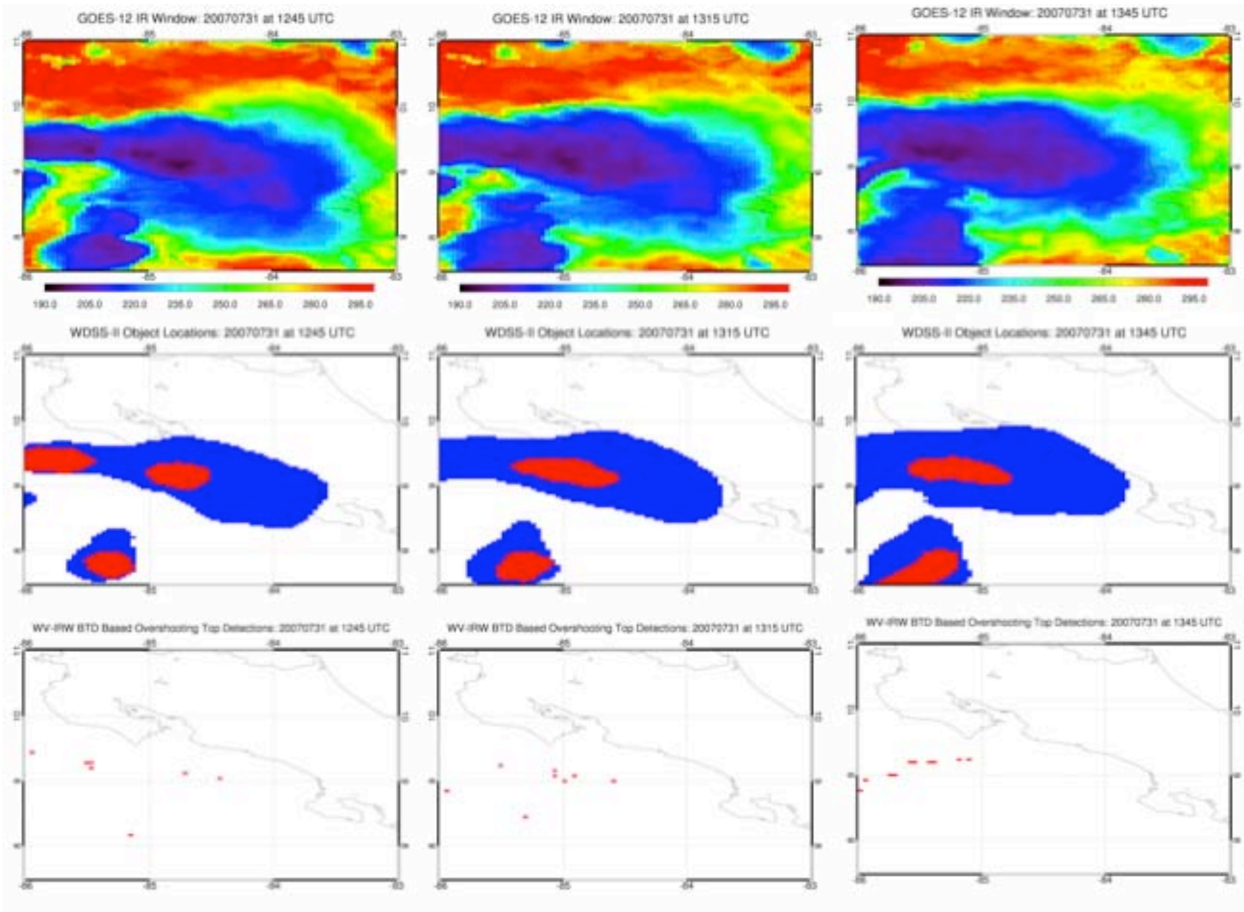

Figure 5: GOES-12 IRW imagery (top row), WDSS-II objects (middle row), and WV-IRW BTD based OT detections (bottom row) at 1245 (left column), 1315 (middle column), and 1345 UTC (right column) on 31 July 2007. WDSS-II objects colored blue represent anvil cloud objects identified with a 225 K IRW BT threshold. WDSS-II objects colored red represent the deep convective area IRW BT ≤ 215 K.

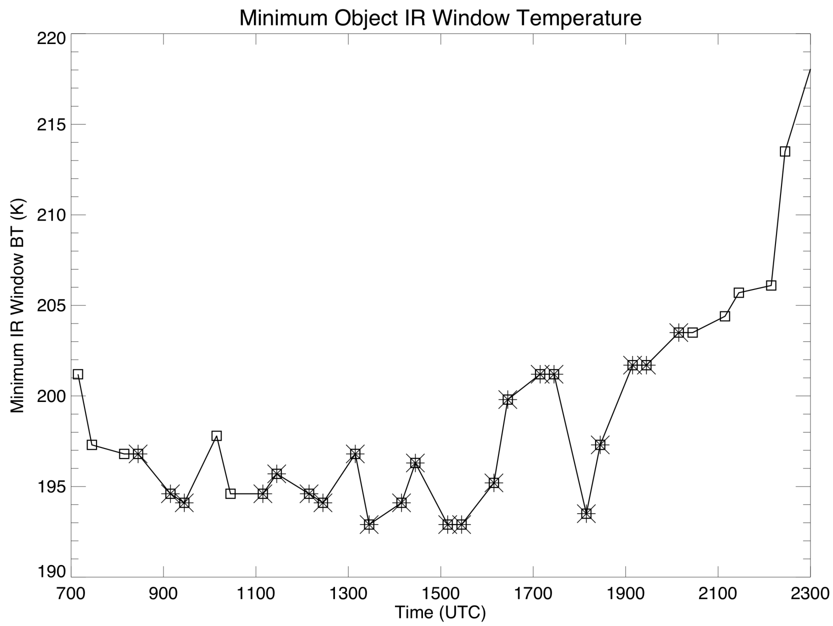

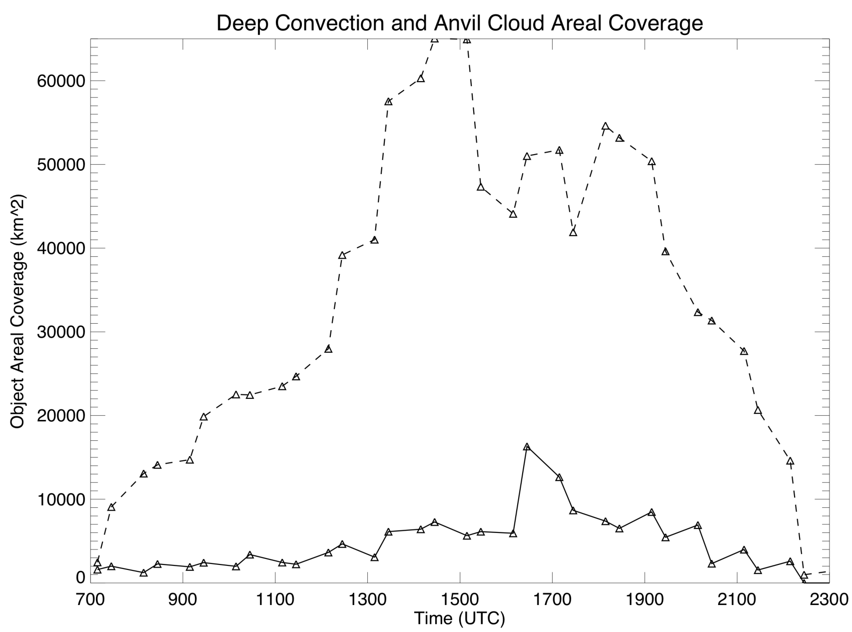

Figure 6: (top) The minimum IRW BT throughout the lifetime of the convective storm complex shown in Figure 5. Asterisks denote the times that OTs were detected within the object. (bottom) The areal coverage of anvil cloud and deep convection for the same object.

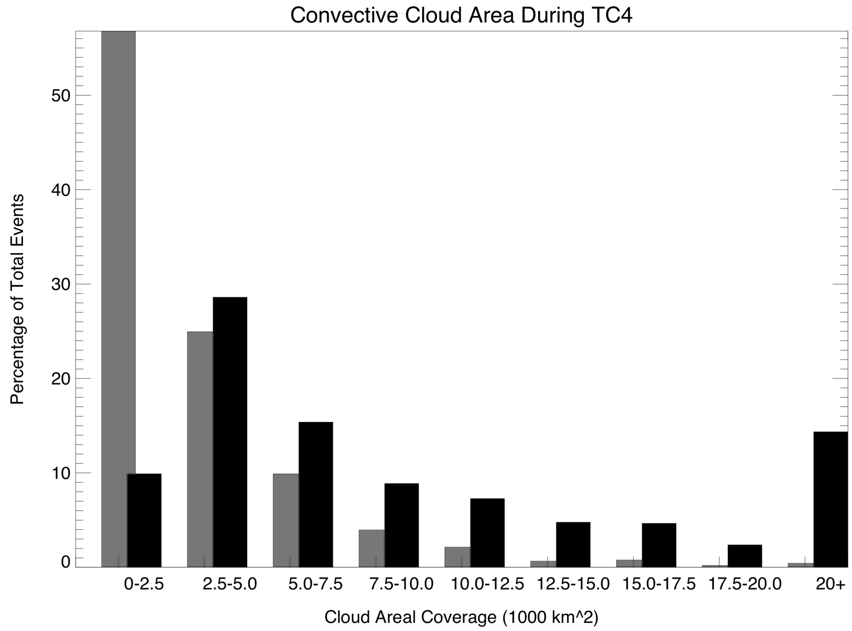

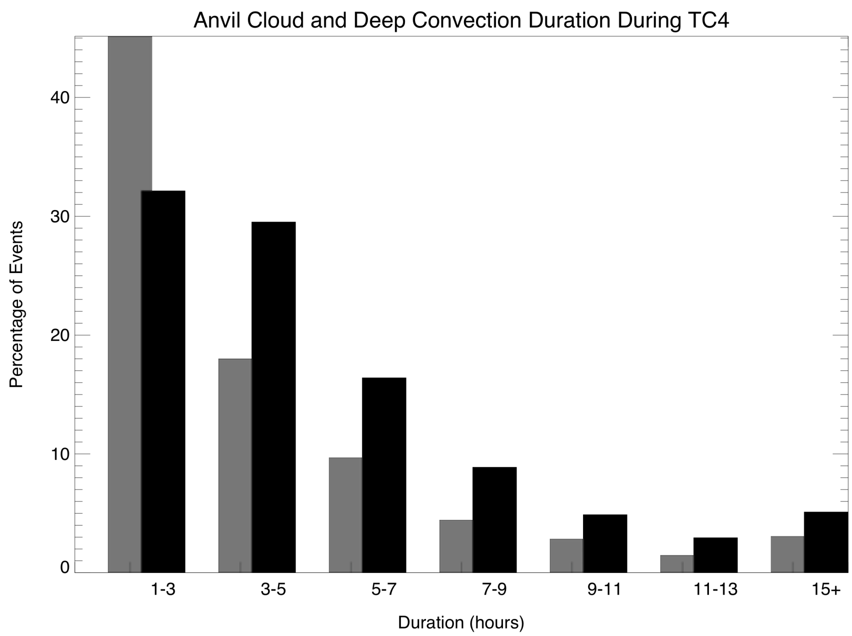

Figure 7: (top) The lifetime of anvil cloud (black bars) and duration of deep convection (grey bars) tracked by the WDSS-II. (bottom) The maximum anvil and deep convective cloud object areal coverage for cloud complexes tracked by the WDSS-II.

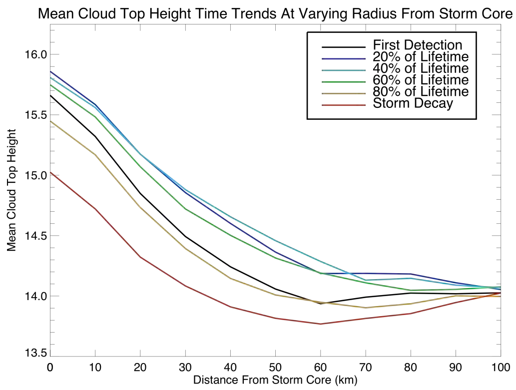

a)

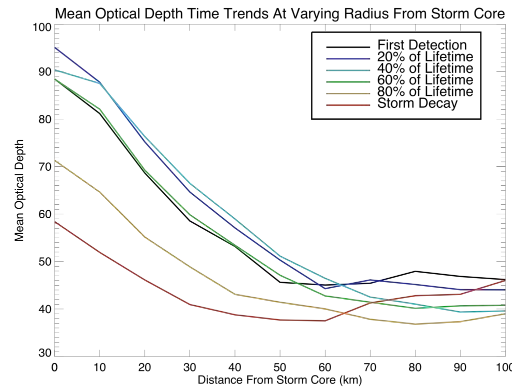

b)

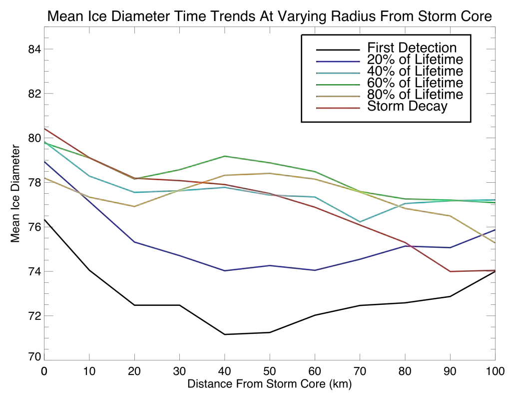

c)

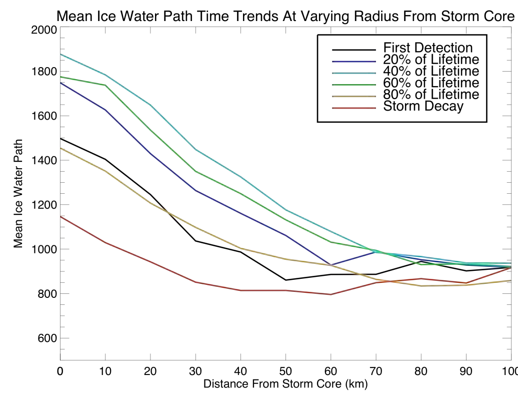

d)

Figure 8: A temporal and spatial variability of the mean a) cloud top height, b) cloud optical depth, c) ice particle diameter, and d) ice water path for a composite of 127-storm complexes during the TC4 field experiment.